Journal of Crystal Growth 338 (2012) 208–213

Contents lists available at SciVerse ScienceDirect

Journal of Crystal Growth

journal homepage: www.elsevier.com/locate/jcrysgro

Influence of travelling magnetic fields on S–L interface shapes of materials with different electrical conductivities

N. Dropka *, Ch. Frank-Rotsch, W. Miller, P. Rudolph

Leibniz Institute for Crystal Growth (IKZ), Max-Born-Str. 2, 12489 Berlin, Germany

ARTICLE INFO

Article history:
Received 8 September 2011
Accepted 9 October 2011
Communicated by A.G. Ostrogorsky
Available online 20 October 2011

Keywords:
A1. Computer simulation
A1. Fluid flow
A1. Solidification
A2. Gradient freeze technique
A2. Single crystal growth

ABSTRACT

Traveling magnetic fields (TMFs) can be used to control the shape of the crystal–melt interfaces at crystal growth from melt. Here, we present the numerical results of a systematic study on the influence of a TMF generated by a KRIST*MAG*® heater-magnet module on the interface curvature of different materials varying in their electrical conductivity in a wide range (5×10^1 to 1.7×10^7 S/m) such as Ge, Si, CdTe, BaF_2 and YAG. Materials were compared in the same design of environment by using results obtained for Ge as a reference. For the rescaling of the growth equipment, non-dimensional criteria were applied. Positive slightly convex crystal–melt interface can be obtained for all materials studied using moderate electrical currents.

1. Introduction

The beneficial role of a traveling magnetic field (TMF) in single crystal growth from melt has been recently reported by different authors [1–3]. Particularly, the application of a KRIST*MAG*® internal heater-magnet module (HMM) for coupled generation of heat and TMF can significantly intensify the melt convection by generated Lorentz forces [4,5]. In the KRIST*MAG*® project it was also shown that TMF can be successfully used in vertical gradient freeze (VGF) growth of Ge crystals to smooth the crystal–melt interface [6,7]. By the optimization of magnetic parameters as phase shift, amplitude and frequency of the AC part of the supplied HMM power, the interface morphology can be modified from an unfavorable concave one to a more promising slightly convex curvature. A significant influence of TMF on the interface shape and segregation in the case of VGF growth of Ge was also obtained by other authors [8,3]. Similar effects on the flow and temperature fields were reported for the Czochralski growth of GaAs (both VCz and LEC) [1,9].

However, the lower the electrical conductivity of the melt the less effective is the induced magnetic field. Thus, for materials with low electrical conductivity of their melt it is much more difficult to achieve the effects aforementioned and the related published data are rare.

Salk et al. showed that a rotational magnetic field can provide a stable flow in a small traveling heater method (THM) environment, dedicated for CdTe growth under μg conditions [10]. Miyazawa et al. showed the principal feasibility of the application of a steady magnetic field at the melt growth of $LiNbO_3$ crystals [11]. However, a very strong induction of 0.5–0.8 T was required. An even higher field of 3 T was used by Wang et al. to affect the interface morphology during growth of (Cd,Zn)Te crystals by THM.

Recently, the first TMF application for improved mixing of a Hg–Cd–Te melt-solution during liquid phase epitaxy (LPE) of (Hg,Cd)Te layers on (Cd,Zn)Te substrates were demonstrated [12]. A remarkable improvement of the layer homogeneity was reported.

The aim of this numerical study is to test the feasibility of applying a TMF via a KRIST*MAG*® HMM at VGF growth of materials differing in a wide range of electrical conductivity from 5×10^1 to 1.7×10^6 S/m. In the study we focus on the control of the interface shape. The interface shape is governed both by the global thermal field and the local melt convection. We like to note that with the HMM the electrical current is used both for heating and for producing the Lorentz forces in the melt. Therefore, there is an upper limit for the electrical current in the coils given by the requirements for the thermal field and thus a limitation for inducing Lorentz forces.

In the following we present a systematic study for five different materials Ge, Si, CdTe, BaF_2, and YAG in a typical VGF furnace equipped with three KRIST*MAG*® HMMs for the generation of required Lorentz forces. We have performed axi-symmetric electro-magnetic and CFD simulations using the commercial code CrysMAS [13,14].

2. Model and methodology

Axi-symmetric numerical calculations were carried out for a typical VGF solidification furnace with one top and one bottom

* Corresponding author.
E-mail address: dropka@ikz-berlin.de (N. Dropka).

0022-0248/$ - see front matter © 2011 Elsevier B.V. All rights reserved.
doi:10.1016/j.jcrysgro.2011.10.007

Nomenclature

D	crucible diameter (m)
F_L	Lorentz force density (N/m^3)
f	frequency of AC current (Hz)
r	growth rate (mm/h)
h	melt and crystal height (m)
ΔH_{LS}	latent heat of solidification (J/m^3)
I	AC current amplitude (A)
q	heat flux (W/m^2)
R	radius of heating coils (m)
T	temperature (K)
Ta	Taylor number (–)
Δz	deflection (mm)
α	thermal expansivity (K^{-1})
δ	skin depth (m)
$\Delta\varphi$	phase shift (°)
λ	thermal conductivity (W/m K)
μ_r	relative magnetic permeability of material ($\mu_r = 1$) for all materials used
μ_0	magnetic permeability of free space (H/m)
ν	kinematic viscosity (m^2/s)
ρ	density (kg/m^3)
σ	electric conductivity (A/V m)

Subscripts

A,B,C	positions in melt and crystal defined in Fig. 1
buoy	buoyancy
CBCF	carbon based isolation
el	electrical
Ge	germanium
m	melting point
X	studied material: Si, CdTe, BaF_2, YAG
HMM	heater-magnet module

standard resistance heater and three KRISTMAG® coil-shaped side heaters. The top and bottom heaters are used for heating only, whereas the side heaters were used for both heating and generating a TMF. We consider an enclosed, electrically insulated crucible with an aspect ratio of $D/h = 2$ for both crystal and melt, where the diameter was $D = 0.113$ m. Fig. 1 shows the simplified model setup.

In order to study the interplay between the flow, thermal and magnetic fields during crystallization we used the commercial code CrysMAS [13,14] and performed the simulations stepwise:

(1) Calculation of the temperature field with a fixed interface and neglecting melt convection.
(2) In this step the heater powers are computed in the manner that at the given three-phase junction of melt, crystal, and crucible the melting-point temperature is reached ($T_A = T_m$, see Fig. 1) and the required temperatures T_B and T_C (positions see Fig. 1) are reached. In addition, the radial temperature gradient in the melt is tried to keep low.
(3) Calculation of pure buoyancy-driven melt flows with interface tracking. Heater powers are adjusted in order to get a nearly flat interface.
(4) Calculation of Lorentz forces for previously selected electromagnetic parameters. Then start from the result of step 2 and include the flow induced by the Lorentz forces.

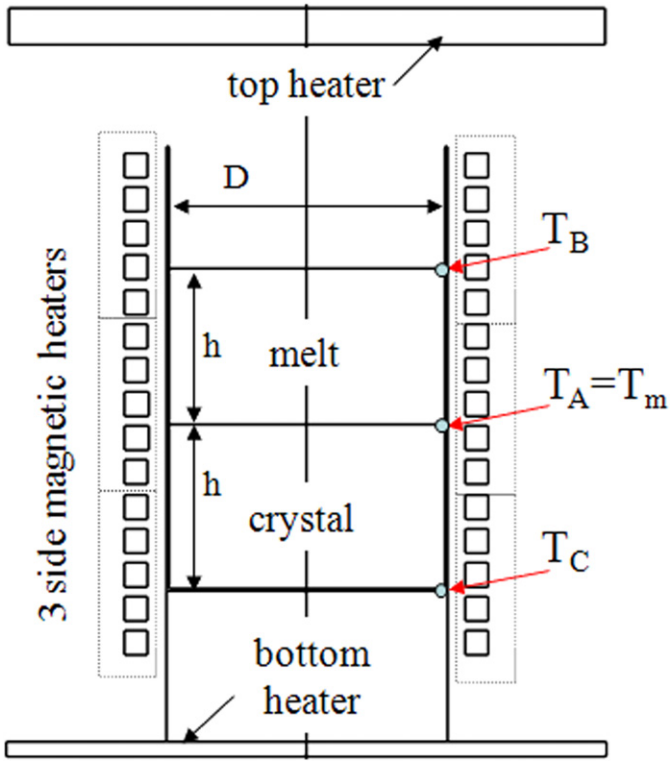

Fig. 1. VGF setup used for numerical modeling.

CrysMAS uses a hybrid scheme: the Navier–Stokes equations are solved on a block-structured mesh for reasons of fast convergence whereas all other equations are solved on an unstructured triangulated grid [13]. The melt domain consists of 2×10^4 mesh elements.

We use the same geometry for all materials and numerical calculations (see Fig. 1). In order to compare materials that significantly differ in their material properties (see Table 1), particularly in their heat and electrical conductivity, some rescaling was performed using Ge as a reference system, which will be described in the following.

For keeping the ratios in heat fluxes in the environment similar for the different materials we replaced the thermal conductivity of real carbon-based isolation used in Ge growth λ^{Ge}_{CBCF} by a virtual conductivity λ^{X}_{iso} according to

$$\lambda^{X}_{iso} = \lambda^{Ge}_{CBCF} \frac{\lambda^{X}_{melt}}{\lambda^{Ge}_{melt}}. \quad (1)$$

The temperature T_C in the solid is computed from the fact that the latent heat produced at the interface has to be removed through the crystal. Therefore, we require a heat flux through the crystal equivalent to the amount of latent heat produced:

$$q_{melt} = r^{X}_{growth} \Delta H^{X}_{LS}. \quad (2)$$

Then, T_C is given via $T_c = T_A - h q_{melt}/\lambda^{X}_{melt}$. The other temperature, i.e. T_B, is given by keeping the same ratio of heat fluxes in melt and solid as for Ge

$$q^{X}_{solid} = q^{X}_{melt} \frac{q^{Ge}_{solid}}{q^{Ge}_{melt}}. \quad (3)$$

In the reference case of Ge the temperature difference in the melt was set to $\Delta T^{Ge}_{melt} = T^{Ge}_B - T^{Ge}_A = 10$ K and in the solid to $\Delta T^{Ge}_{solid} = T^{Ge}_A - T^{Ge}_C = 40$ K.

Table 1
Material properties used in this study.

Property	State	Ge	Si	BaF_2	CdTe	YAG
λ_{melt} (W/m K)	Melt	39	67	0.2	3	4
λ_{solid} (W/m K)	Solid	17	22	2	1.5	8
ΔH_{LS} (J/m^3)		4×10^9	4.6×10^9	1.8×10^9	1.3×10^9	1.96×10^9
σ_{el}^{melt} (S/m)	Melt	1.7×10^6	1.2×10^6	3.92×10^2	1.05×10^4	6×10^2
σ_{el}^{solid} (S/m)	Solid	1.6×10^6	5×10^4	3.92×10^2	8.5×10^3	5
ν (m^2/s)	Melt	1.4×10^{-7}	3.4×10^{-7}	2.48×10^{-6}	4.5×10^{-7}	1.3×10^{-5}
α (K^{-1})	Melt	1.1×10^{-4}	1.1×10^{-4}	2×10^{-5}	1.45×10^{-4}	1.8×10^{-5}
ρ (kg/m^3)	Melt	5500	2530	4830	5640	4300
r (mm/h)		3	9	1	1	0.8
T_m (K)		1210	1685	1624	1365	2243

Table 2
Electro-magnetic parameters required for electro-magnetic similarity of different materials using $\delta = 6.02\times10^{-2}$ m and $T_a = 7.99\times10^{-7}$.

Parameter\material	Ge	Si	CdTe	BaF_2	YAG
f (Hz)	41	58	6657	1.79×10^5	1.17×10^5
I (A)	150	256	507	2588	11,692

In principle, for electro-magnetic similarity the skin depth should be identical for all materials studied

$$\delta_X = \frac{1}{\sqrt{\mu_r\mu_0\sigma_X\pi f_X}}. \quad (4)$$

Due to the large differences in electrical conductivity Eq. (4) would give rather large frequencies for CdTe, YAG, and BaF_2 even if the frequency for Ge is rather low (see Table 2). Frequencies beyond 1000 Hz are difficult to realize in resistant heaters and therefore we restrict to $f \le 1000$ Hz in the study on the influence of TFM on the crystal–melt interface.

The influence of TMF on the convection can be estimated by the magnetic Taylor number

$$\mathrm{Ta}_X = \frac{\pi f_X \sigma_X}{\rho_X \nu_X^2}\left(\frac{I_X\mu_0 R_{coil}}{2}\right)^2. \quad (5)$$

Once again, in principal one can obtain the electrical current I from Eq. (5) for a given Taylor number. However, the current exceeds feasible values for BaF_2 and YAG (see Table 2). Please, keep in mind that this electric current is not only used for producing Lorentz forces but also for heating. High currents will result in overheating and are therefore not usable. In our study of interface deflection we restrict to currents up to $I = 500$ A.

Based on the preceding assumptions, the electro-magnetic parameters of TMF were studied in the following ranges:

1. Phase shift $\Delta\phi = \pm30^\circ, \pm60^\circ, \pm120^\circ$. The phase shift in the side heaters was counted from top to bottom.
2. Frequency Ge: $f = 20$–400 Hz, Si: $f = 28$–567 Hz, CdTe: $f = 500$–1000 Hz, BaF_2: $f = 500$–1000 Hz, YAG: $f = 200$–1000 Hz.
3. Electrical current Ge: $I = 70$ A, Si: $I = 60$ A, CdTe: $I = 150$ A, BaF_2 $I = 500$ A, YAG: $I = 500$ A.

3. Results and discussion

We have performed a first set of runs with a phase shift of 30° and tuned both frequency and electrical current for Si, CdTe, and BaF_2 in order to get Lorentz forces of the same order as for the reference system of Ge with $I = 70$ A and $f = 50$ Hz. The Lorentz force density distributions for Ge and Si for one pair of frequency and phase shift ($f = 50$ Hz, $\Delta\phi = 30^\circ$) are given in Fig. 2. Due to their similar physical properties, the obtained fields and skin depths are also similar being $\delta = 0.055$ m and $\delta = 0.065$ m for Ge and Si, respectively. Such skin depths are of the order of the radius of the crucible. Positive $\Delta\phi$ gives upwards directed Lorentz forces

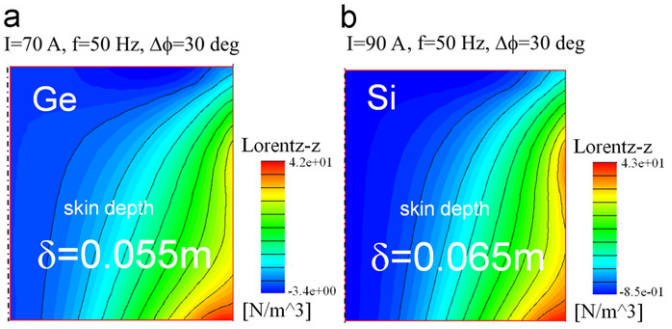

Fig. 2. Vertical component of Lorentz force density in (a) Ge melt ($I = 70$ A, $f = 50$ Hz, $\Delta\phi = 30^\circ$ and (b) Si melt ($I = 90$ A, $f = 50$ Hz, $\Delta\phi = 30^\circ$).

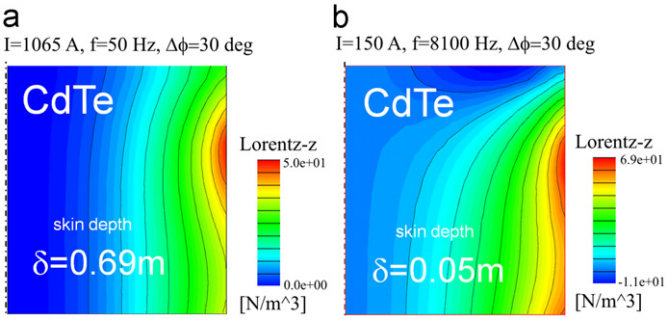

Fig. 3. Vertical component of Lorentz force density distribution in CdTe melt. Left: $I = 1065$ A, $f = 50$ Hz, $\Delta\phi = 30^\circ$ and (b) $I = 150$ A, $f = 8.1$ kHz, $\Delta\phi = 30^\circ$.

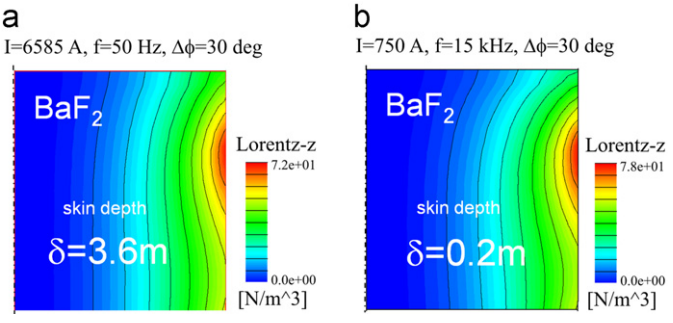

Fig. 4. Vertical component of Lorentz force density distribution in BaF_2 melt for (a) $I = 6585$ A, $f = 50$ Hz, $\Delta\phi = 30^\circ$ and (b) $I = 750$ A, $f = 15$ kHz, $\Delta\phi = 30^\circ$.

with maximum magnitude at the crucible rim in the vicinity of crystal–melt interface. Opposite effect appears at $\Delta\phi < 0^\circ$, i.e. downwards directed forces with maximum magnitude at the rim close to the melt-free surface. The magnitude of F_L increases with increasing frequency and current magnitude, but it is dependent on the inverse of phase shift. In particular, $F_L \propto I^2$ and a change in the electrical current results in different values of F_L but not in their distribution or their direction. These can be tuned by the frequency f and partly by the phase shift $\Delta\phi$.

If we apply the same frequency and phase shift ($f = 50$ Hz, $\Delta\phi = 30^\circ$) to CdTe melt having an electrical conductivity two orders of magnitude lower than Ge, the skin depth becomes 10 times larger and exceeding the radius of the melt. More important is the need of a much larger current amplitude ($I = 1065$ A) to reach F_L in the same order of magnitude like in the reference case (Fig. 3, left). Note, such a high electrical current would generate strong thermal effects in the melt and would damage the imposed temperature distribution. An alternative way to generate Lorentz forces of desired intensity and distribution in CdTe is to increase the frequency from $f = 50$ Hz up to $f = 8.1$ kHz while keeping the current low (Fig. 3, right).

Table 3
Skin depth of Lorentz forces as a function of frequency for BaF_2.

f (Hz)	50	15,000	200,000
δ (m)	3.6	0.2	0.057

For materials with very low electrical conductivity of the melt like BaF_2 and YAG, the required electrical currents for low frequencies are even more pronounced (see Fig. 4, left). In addition, the skin depth of $\delta = 0.055$ m can be reached only with a very high frequency (see Table 3), which is beyond a practical realization. Therefore, we chose $f = 15$ kHz and $I = 750$ A in the case of BaF_2 to have process parameters, which can be applied in real experiments. Because the skin depth is still larger than the radius of the melt there is not much difference in the distribution

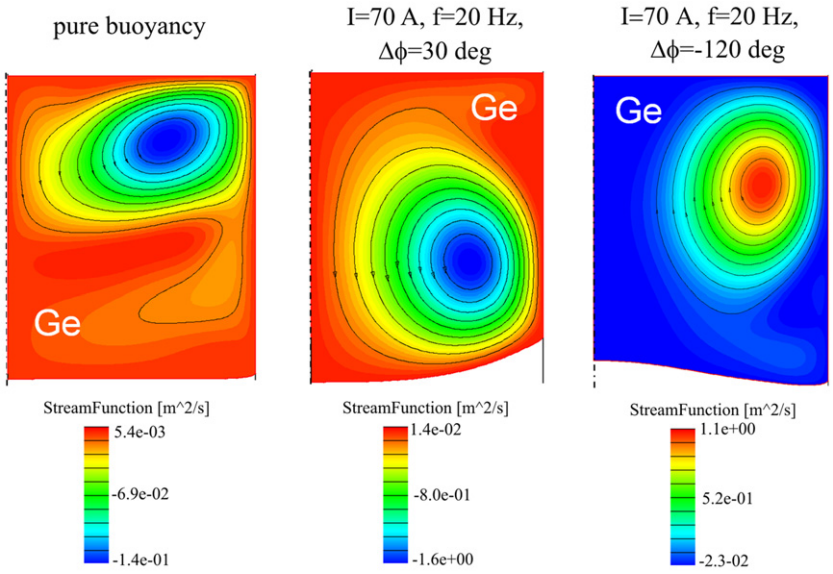

Fig. 5. Flow patterns and interface morphology for Ge.

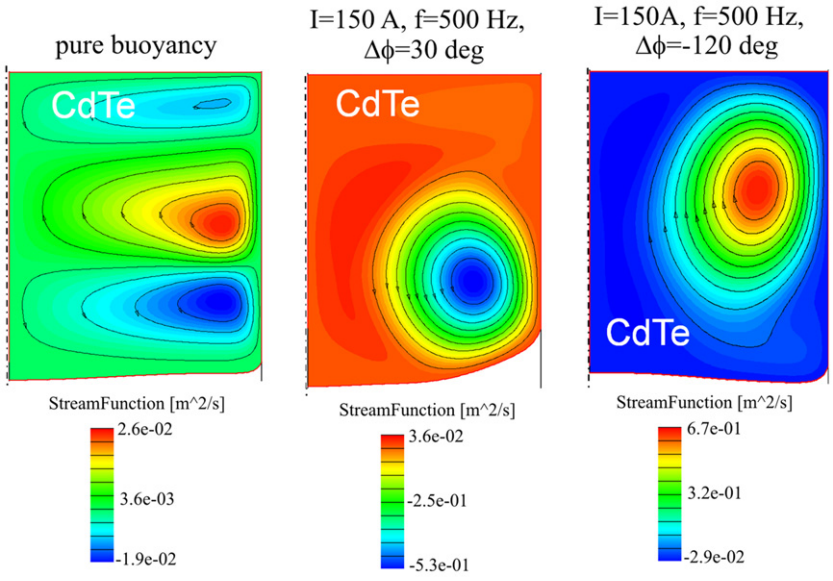

Fig. 6. Flow patterns and interface morphology for CdTe.

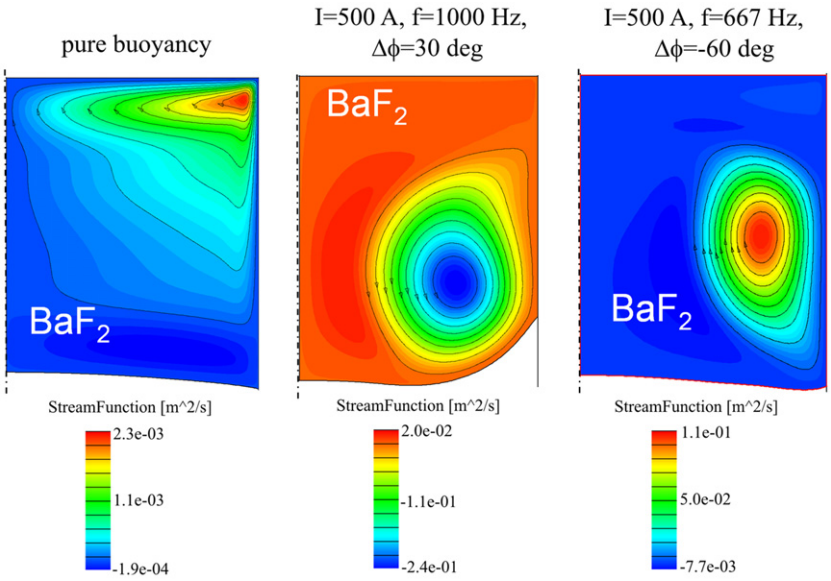

Fig. 7. Flow patterns and interface morphology for BaF_2.

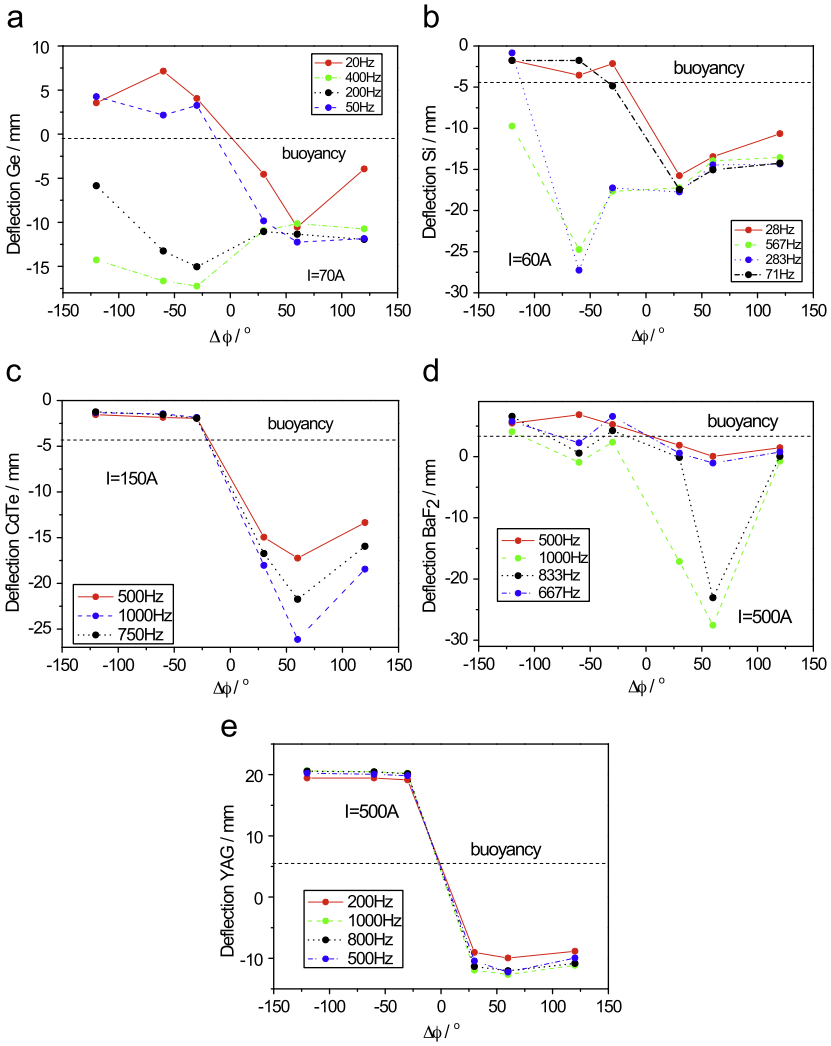

Fig. 8. Interface deflection for different materials, frequencies and electrical currents as a function of the phase shift $\Delta\phi$. (a) Ge, (b) Si, (c) CdTe, (d) BaF_2, (e) YAG.

of the vertical Lorentz force densities between the right and the left picture in Fig. 4.

In the case of CdTe the picture is different and the distribution of the vertical Lorentz force densities becomes similar to those of Ge and Si for $\delta = 0.05$ m (compare Fig. 3, right and Fig. 2).

Now, we will present the results for the influence of TFM on the interface deflection. The interface deflection Δz is measured at the symmetry axis with respect to the three phase junction (melt/crystal/crucible). For pure buoyancy convection the interface shape varies from slightly concave ($\Delta z < 0$) in the case of Ge, Si, and CdTe to slightly convex ($\Delta z > 0$) for BaF_2 and YAG (see left side in Figs. 5–8). For the two latter materials heat conductivity is higher in the solid than in the melt and thus latent heat can be removed in the center more efficiently than in the case of the other materials, where the heat conductivity is lower in the solid than in the melt. At this point we like to remind the reader that thermal optimization for each material was not subject of this investigation.

From Fig. 8 it can be clearly seen that for all materials it is possible to have a significant influence on the convection and the thermal field when choosing realistic process parameters. A TMF downwards ($\Delta\phi < 0$) always increase the convexity of the interface due to the establishing of one convection role with downward flow at the crucible (see right sides in Figs. 5–7). The opposite happens for a TMF upwards ($\Delta\phi > 0$): the interface is strongly bending upwards towards the crucible (see middle in Figs. 5–7).

In all cases the process could be improved with respect to interface deflection: the negative values (concave interface) can be reduced (Si, CdTe) or changed in two positive ones (convex interface) for Ge, the convexity in the case of BaF_2 can be reduced to get a flatter interface.

The YAG system is very sensitive to changes in melt convection because of its high Prandtl number ($Pr \approx 10$) in comparison to BaF_2 ($Pr \approx 0.2$) and CdTe ($Pr \approx 0.4$). A fine tuning of the process parameters is necessary for optimizing the interface shape.

4. Conclusions

For Ge, Si, CdTe, BaF_2 and YAG melts with electrical conductivity in the range from 5×10^1 to 1.7×10^6 S/m Lorentz force densities being comparable or larger than the buoyancy force densities can be achieved by using moderate electrical currents. For materials with low electrical conductivity, higher frequencies should be used in order to keep the electrical current in a range attractive for commercial applications. In general, positive slightly convex deflection of the crystal–melt interface can be obtained for all studied materials. Our calculations show that TMF generated inside a VGF equipment with KRISTMAG® HMM is a promising tool for interface control and related improvement of crystal growth process not only for materials with high electrical conductivity but also for such ones showing low electrical conductivities.

References

[1] P. Rudolph, M. Czupalla, B. Lux, LEC growth of semi-insulating GaAs crystals in traveling magnetic field generated in a heater–magnet module, Journal of Crystal Growth 311 (2009) 4543–4548.
[2] P. Rudolph, Travelling magnetic fields applied to bulk crystal growth from the melt: the step from basic research to industrial scale, Journal of Crystal Growth 310 (2008) 1298–1306.
[3] V. Galindo, I. Grants, R. Lantzsch, O. Pätzold, G. Gerbeth, Numerical and experimental modeling of the melt flow in a traveling magnetic field for vertical gradient freeze crystal growth, Journal of Crystal Growth 303 (2007) 258–261.
[4] N. Dropka, W. Miller, U. Rehse, P. Rudolph, F. Büllesfeld, U. Sahr, O. Klein, D. Reinhardt, Numerical study on improved mixing in silicon melts by double-frequency TMF, Journal of Crystal Growth 318 (1) (2011) 275–279.
[5] N. Dropka, W. Miller, R. Menzel, U. Rehse, Numerical study on transport phenomena in a directional solidification process in the presence of travelling magnetic fields, Journal of Crystal Growth 312 (8) (2010) 1407–1410.
[6] C. Frank-Rotsch, P. Rudolph, Vertical gradient freeze of 4 inch Ge crystals in a heater-magnet module, Journal of Crystal Growth 311 (2009) 2294–2299.
[7] C. Frank-Rotsch, D. Jockel, M. Ziem, P. Rudolph, Numerical optimization of the interface shape at the VGF growth of semiconductor crystals in a traveling magnetic field, Journal of Crystal Growth 310 (2008) 1505–1510.
[8] R. Lantzsch, I. Grants, O. Pätzold, M. Stelter, G. Gerbeth, Vertical gradient freeze growth with external magnetic fields, Journal of Crystal Growth 310 (2008) 1518–1522.
[9] O. Klein, C. Lechner, P.-E. Druet, P. Philip, J. Sprekels, C. Frank-Rotsch, F.-M. Kießling, W. Miller, U. Rehse, P. Rudolph, Numerical simulation of Czochralski crystal growth under the influence of a traveling magnetic field generated by an internal heater-magnet module (HMM), Journal of Crystal Growth 310 (2008) 1523–1532.
[10] M. Salk, M. Fiederle, K.W. Benz, A.S. Senchenkov, A.V. Egorov, D.G. Matioukhin, CdTe and $CdTe_{09}Se_{0.1}$ crystals grown by the travelling heater method using a rotating magnetic fielddte09se0.1 crystals grown by the travelling heater method using a rotating magnetic field, Journal of Crystal Growth 138 (1994) 161–167.
[11] Y. Miyazawa, S. Morita, H. Sekiwa, Flow in oxide melts in a high magnetic field, Journal of Crystal Growth 166 (1996) 286–290.
[12] H. Bitterlich, C. Frank-Rotsch, W. Miller, U. Rehse, P. Rudolph, Homogeneous TMF melt-solution mixing during dipping LPE of (Hg,Cd)Te layers, Journal of Crystal Growth 318 (2011) 1034–1038.
[13] J. Fainberg, D. Vizman, J. Friedrich, G. Mueller, A new hybrid method for the global modeling of convection in CZ crystal growth configurations, Journal of Crystal Growth 303 (2007) 124–134.
[14] M. Kurz, A. Pusztai, G. Müller, Development of a new powerful computer code CrysVUN++ especially designed for fast simulation of bulk crystal growth processes, Journal of Crystal Growth 198/199 (1999) 101–106.